Journal of Geological Remote Sensing 2023 1(1);90- 103

Graduate University of Advanced Technology

Journal of Geological Remote Sensing

Journal homepage: https:// jgrs.kgut.ac.ir

Iranian Geological Remote Sensing Society

Structure, Alteration, and Mineralization Analysis in Central Kerman Copper Belt using Remote Sensing Data

Reyhaneh Zandi *

M.Sc. student, Valiasr University of Rafsanjan, Rafsanjan, Iran

Article Info

Keywords:
porphyry copper geological structures logical algorithm method
Fry's analysis
Lineament density analysis
hydrothermal alteration

Abstract

This research analyzes the relationship between geological structures, alteration, and mineralization at the porphyry copper deposits in the central part of the Dehaj- Sarduiyeh magmatic belt, located in Kerman province. To extract fractures, non-directional and directional filters were implemented on the Sentinel 2, Landsat 9 satellite images, and the digital elevation model (DEM). The spatial distribution of the significant deposits and structures analysis were done using Fry and lineament density methods. In addition, hydrothermal alteration zones were enhanced by the implementation of the logical algorithm method on the Advanced Space-borne Thermal Emission and Reflection Radiometer (ASTER) images. The comparison of the structural analysis with the discriminated hydrothermal alteration map showed that there is a logical relationship between the lineament density and the position of the copper deposits. The rose diagram of the fractures shows the northwest-southeast and northeast-southwest trend, which is consistent with the rose diagram trend of the porphyry copper deposits in the region. The results of this research showed that Fry's method can be used for structural analysis in the exploration of porphyry copper deposits.

*Corresponding author.
Email: zandir894@gmail.com

https://doi.org/10.48306/jgrs.2024.409225.1004
Received 30 July 2023; Received in revised form Aug. 2023; Accepted 12 Oct. 2023
Available Aug 2023

1. Introduction

The purposive stepwise exploration plays a key role in lowering mineral exploration costs. Satellite image processing can greatly contribute to the cost reduction of mineral exploration especially in the preliminary detection and prospecting. Remote sensing data have a high potential to identify alteration regions of deposits, thereby detecting minerals (Sabins, 1999). Linear structures such as faults and fractures have a central role in magmatic mass positions, extension, and distribution of alteration zones as well as mineralization (Berger and Drew, 1997). Fractures, especially faults, are essential determinants in the formation of mineral deposits. The identification of structural elements in a region can profoundly help detect and explore minerals, as these elements may be candidate sites for magma intrusions and then mineralization. Argillic, phyllic, potassic, and propylitic alterations are considered major alterations that can be detected through remote sensing in regions affected by hydrothermal fluids. According to Figure 1, these alteration zones typically have particular minerals characterized by spectral features such as calcite, epidote, and chlorite (propylitic zone), kaolinite and alunite (argillic zone), muscovite and illite (phyllic zone), and orthoclase, biotite, and quartz (potassic zone). Moreover, these minerals have drawn significant attention in the remote sensing literature due to unique spectral characteristics in the visible and near-infrared (VNIR) and short-wave infrared (SWIR) regions (Rowan and Mars 2003, Mars and Rowan, 2006).

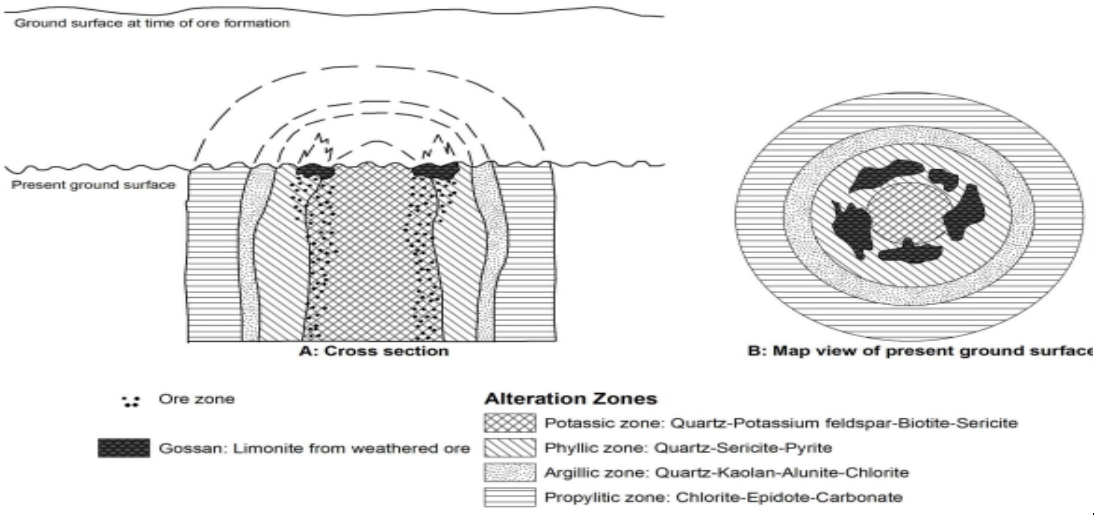

Figure 1. The model of hydrothermal alteration zones related to porphyry copper deposits, including potassic, phyllic, argillic, and propylitic alterations (Sabins, 1999).

Several hyper- and multispectral scanners, *e.g.*, Hyperion, ASTER, and Landsat, were employed to enhance alteration zones (Honarmand et al., 2013; Hosenjanizadeh et al., 2014; Pour AB and Hashemi 2015., Bedini 2017., Govil et al. 2018., Shirmard et al., 2020). The multispectral ASTER sensor which launched in December 1999, has shown great capabilities in the enhancement of alteration zones due to the relatively more band in the SWIR

region. This sensor contains fourteen bands in the VNIR, SWIR, and thermal IR (TIR) ranges. ASTER images have good spectral and spatial resolutions and can effectively enhance hydrothermal alteration zones. Many studies have analyzed alteration zones through remote sensing based on ASTER data all over the world, especially in the case study area (Mars and Rowan, 2006., Hosseinjanizadeh et al., 2014; Shahriari et al., 2015; Honarmand et al., 2018; Yousefi et al., 2018; Wang et al., 2020 Beygi et al., 2021). In addition, determining lineaments including faults and fractures can be used as an exploratory key in mineral exploration (Alizadeh et al., 2015; Molaei et al., 2020). Therefore, it is essential to identify the relationships between linear structures and hydrothermal alterations which may, in turn, lead to the detection of deposits. Fry analysis as a complementary method in structural geological studies can be used to study the distribution of mineralization in a region and its relationship with linear structures (Yaghoubpour et al., 2006; Ahmadfaraj, et al. et al., 2019; Shirazi et al., 2022). Previous works conducted in the case study area rarely evaluated the relationships of structures and fractures with hydrothermal alterations. To the best of the authors' knowledge, the distribution of deposits using the Fry pattern in the study area has not been studied yet. The present study aimed to analyze the density of structural fractures (faults) by the lineament density, evaluate the distribution of the deposit using the Fry method, and identify relationships between faults, alterations, and mineralization through remote sensing data in the central part of Kerman Copper Belt.

2.Study area

The study area is situated in the southern part of the central Iranian Urumieh–Dokhtar magmatic belt (UDMB) in Kerman province, Iran (Figure 2(a)). This area encompasses the 1:100,000 maps of Pariz, Chahargonband, and Rafsanjan 1 and 2, and is located in the central part of the Kerman Copper Belt (Figure 2). The UDMB also known as the Sahand– Bazman Belt (Vialon et al., 1972), is among the major metallogenic provinces of copper in the world. The UDMB is part of the Alpine–Himalayan orogenic belt that stretches from Western Europe to Turkey, Iran, and Western Pakistan. This magmatic arc contains massive quantities of intrusive and volcanic rocks. Copper magmatic and mineralization activities along the UDMB occurred from the Eocene to the end of the Miocene (Shafiei et al., 2009), forming most of the copper deposits and prospects. The Kerman copper metallogenic belt, which is also known as the Dehaj–Sarduieh copper belt (Dimitrijevic, 1973) and Kerman Cenozoic Magmatic Arc (KCMA), is the most important part of the UDMB. This belt has a length of 500 km and a width of 80 km and stretches in the northwest-southeast direction in the southern margin of the Central East Iranian Microcontinent (CEIM). Dehaj- Sarduiyeh belt has a thickness of approximately 15 km of acidic to moderate volcanic rock and basic Eocene rock penetrated by Oligo–Miocene intrusive rocks (Dimitrijevic, 1973). Eocene and early Oligocene volcano-sedimentary rocks include; Paleocene-lower Eocene sedimentary rocks with Flysch facies, Bahr Aseman lower-middle Eocene volcanic-plutonic complex, a sedimentary complex with middle Eocene Flysch facies, Razak middle-upper Eocene volcano-sedimentary sequence, and Hezar upper Eocene-middle Oligocene volcanic complex (Dimitrijevic 1973., Shafiei 2010). The largest portion of the Kerman Cenozoic magmatic rocks belong

to the Eocene volcanic complex, with 6600 km^3 of volcanic rock in the form of magma and pyroclastic rock. Structural features have played a key role in the replacement of intrusive masses and deposits in the Kerman metallogenic belt. In the Kerman copper belt, fault structures mostly have northwest-southeast trending and conform to the direction of intrusive masses and alteration zones (Shafiei et al., 2009). This region is characterized by the presence of several porphyry and vein copper mineral deposits and many occurrences. Porphyry types like Sarchesmeh, Darehzar, and Kohpanj, are more important and are located mainly in the post-Eocene intrusive bodies in the Eocene volcanic–sedimentary complex. The vein-type mineralization has been found both in the intrusive and in the volcanic rocks and has been controlled by faults with different trends (Dimitrijevic, 1973; Hosseinjanizadeh and Honarmand 2017). The Eocene volcano-sedimentary rocks, especially the Razak series, account for the main rock type in the region Figure 2(c). Intrusive rocks have penetrated the complex in the form of several Oligo–Miocene and Paleocene stocks and dikes, leading to extensive hydrothermal alterations and copper deposits of porphyry and vein types. The Eocene volcanic complex includes a set of magmas with a combination of trachyandesite, andesite, andesite-basalt, and, rarely, olivine-basalt (Honarmand, 2012).

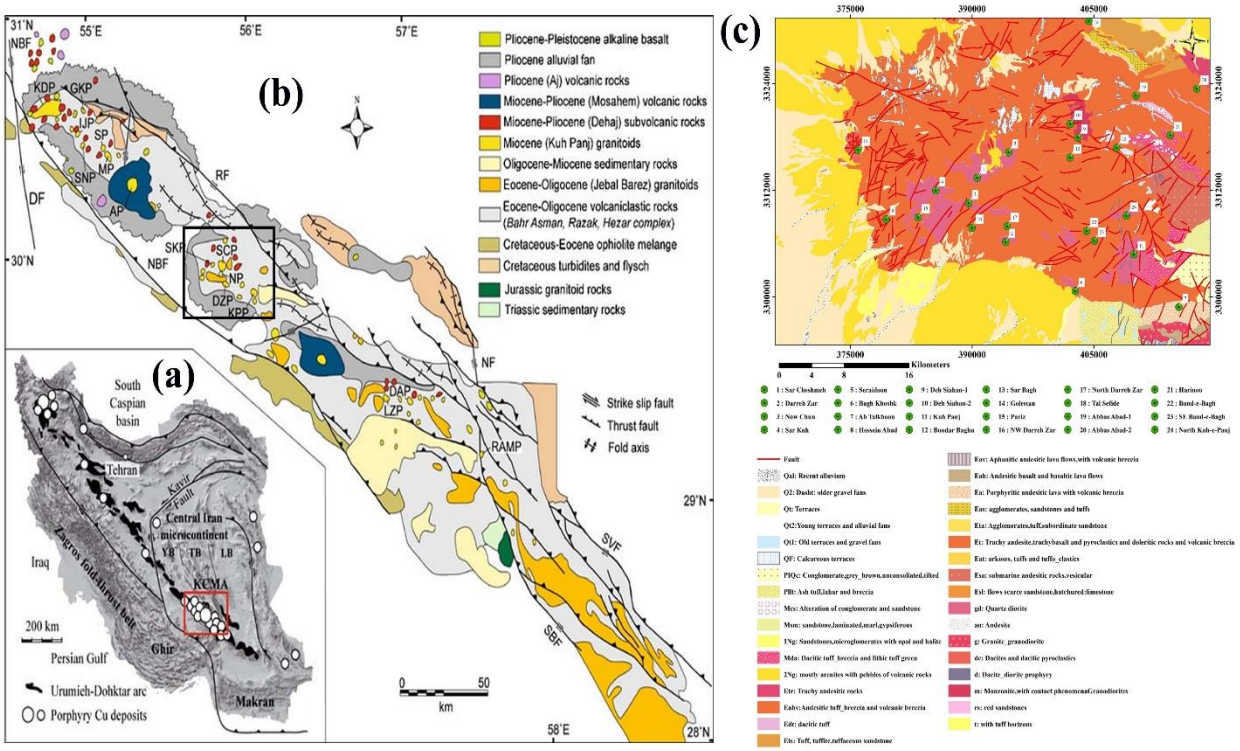

Figure 2. (a) simplified map of the KCMA,(Honarmand, 2012), (b) case study region in the UDMB, Iran (compiled from Dimitrijevic (1973), Saric and Mijalkovic (1973), Stocklin and Nabavi, (1973), Dercourt et al., (1986), Emami et al., (1993), and Samani (1998), and (c) 1:100000 geological map of the case study region with porphyry copper deposits.

3. Materials and Methods

The ASTER_ level 1B data was used to identify the hydrothermal alteration minerals through the ENVI Interactive Data Language (IDL) and the logical algorithm in this study. Landsat 9 (OLI_2), Sentinel_2A, and digital elevation model data were also used to highlight faults and lineaments. In addition, Fry's analysis was implemented to investigate the main trends in the spatial pattern of deposits and their spatial relationships with structures. The flowchart of the research method is shown in Figure 3.

3.1. Enhancement of Alteration Zones

Characteristic minerals of argillic alteration include alunite with diagnostic absorption features at 2.165 μm corresponding to Band 5 of ASTER and kaolinite with characteristic absorption at 2.165 and 2.2 μm corresponding to Band 5 and 6 of ASTER. The characteristic minerals of phyllic alteration include muscovite and illite with diagnostic absorption features at 2.2 μm corresponding to Band 6 of ASTER. The characteristic minerals of propylitic alteration include epidote and chlorite with diagnostic absorption feature at 2.3 μm corresponding to band 8 of ASTER. To enhance hydrothermal alterations zones in the study area, a set of band ratios was employed to define an algorithm for discrimination of alteration minerals including; chlorite and epidote as indicators of propylitic alterations, alunite and kaolinite as characteristic minerals of argillic and advanced argillic alteration, and illite and muscovite characteristic mineral for phyllic alteration through the Interactive Data Language (IDL) and the logical algorithm (Mars & Rowan, 2006).

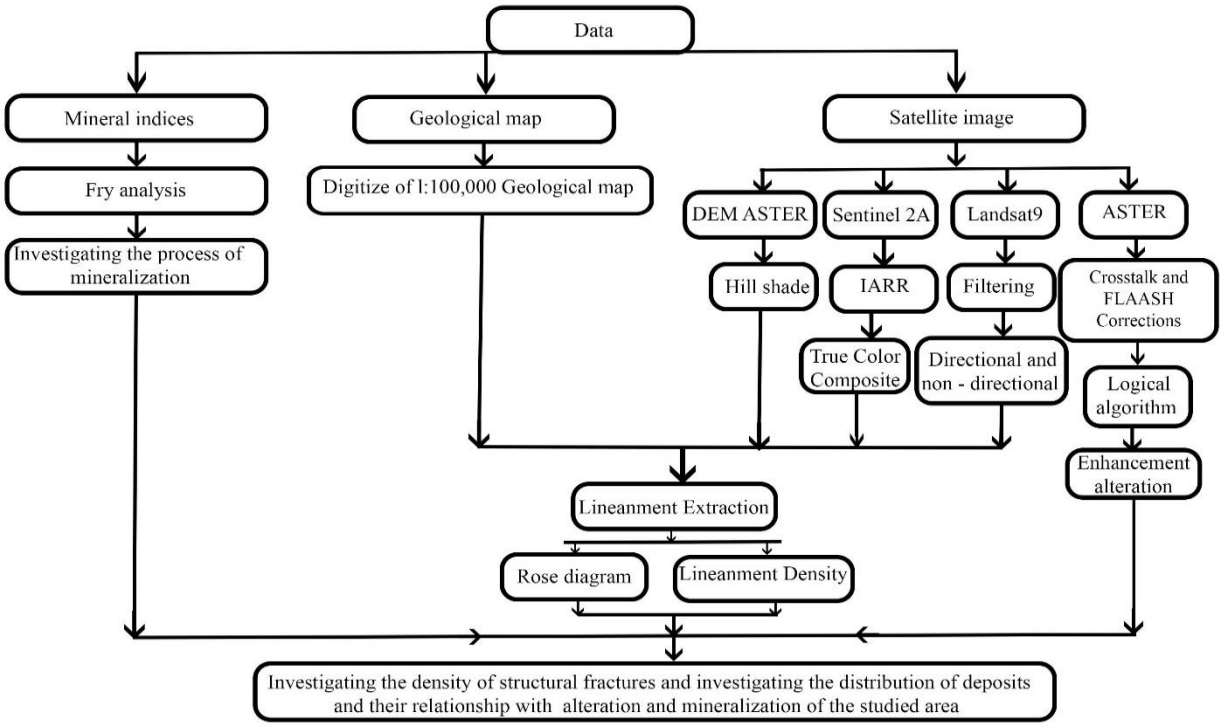

Figure 3. Flowchart of the study procedure applied in this investigation

Table 1. Algorithms adopted to detect alterations (Mars & Rowan, 2006).

Alteration	Algorithm
Argillic (kaolinite, alunite)	((float(b3)/b2) le 1.41) and (b4 gt 260) and ((float(b4)/b5) gt 1.2087) and ((float(b5)/b6) le 1.025) and ((float(b7)/b6) ge 1.064)
Phyllic (illite, muscovite)	((float(b3)/b2) le 1.41) and (b4 gt 260) and ((float(b4)/b6) gt 1.210) and ((float(b5)/b6) gt 1.025) and ((float(b7)/b6) ge 1.064)
Propylitic(chlorite, epidote)	((float(b3)/b2) le 1.41) and b4 gt 260 and (float(b6)/ b8 gt 1.112) and (b5 gt b6) and (b7 gt b8) and (b9 gt b8)

3.2. Lineament Extraction

Landsat 9 (OLI_2), Sentinel-2A, and digital elevation data were utilized to enhance lineaments and faults. Table 2 provides the Characteristic bands of OLI and Sentinel-2. Landsat 9, which launched in September 2021, has radiometric and geometric advantages over the earlier Landsat generations (NiroumandJadidi et al., 2022). OLI_2 images captured on 4 August 2022 were used in this study. Since the radiometric and atmospheric correction for OLI_2 images of Landsat 9 Collection 2 Level-2 were implemented automatically by the manufacturer, there is no requirement to correct these data. Initially, to enhance spatial resolution, the VNIR-SWIR of Landsat 9 bands were sharpened with the panchromatic band, which has a spatial resolution of 15 meters. Then, a non-directional filter (High Pass) and directional filters (Directional) at 45 and 135 degrees were applied to the pan-sharped images to highlight lineaments using ENVI 5.6 software.

The Shuttle Radar Topography Mission (SRTM) is spearheaded by NASA, the National Geospatial-Intelligence Agency (NGA), and the German and Italian space agencies and covers nearly the entire earth (Gorokhovich and Voustianiouk, 2006). The SRTM data were collected on an 11-day mission in February 2000. They were provided with spatial resolutions of 30 and 90 m. The digital elevation model (DEM) of SRTM had 30-m elevation data including three images captured on 23 September 2014. The digital elevation model (DEM) data with a 30-meter resolution was used to create a hillshade of the area. Subsequently, an RGB composite was created from Landsat directional filters at 45 and 135 degrees, the hillshade image to easily identify the lineaments.

The Sentinel 2A satellite, which was launched on 23 January 2015, provides remote sensing data in 13 spectral bands in VNIR and SWIR regions. Sentinel 2 contains four visible and near-infrared (NIR) bands with a spatial

resolution of 10 meters, six SWIR and red-edge bands with a spatial resolution of 20 meters, and three bands with a spatial resolution of 60 meters. In this study, Sentinel 2A Level-1C images on August 21, 2019, acquired from the Copernicus open- access website, were used. The internal average relative reflectance correction (IARR) method was performed on Sentinel 2 data to convert radiation to relative reflectance. (Ven der Werff and Ven der Meer, 2016). The faults in the study area were manually and accurately extracted using Sentinel bands with 10 m spatial resolution, specifically the 234 true color composition, and 1: 100,000 geological map through ARC GIS 10.8.2 software.

Finally, a supervised map of the faults and lineaments in the area was prepared by integrating the extracted lineaments of Landsat, Sentinel, and 1:100000 geological map. For the initial analysis of lineament trends, rose diagrams based on the method proposed by Robson (1994) were created using Rock Work software.

ASTER Band N.	Band Center (µm)	Spectral resolution (m)	Sentinial-2 Band N.	Band Center (µm)	Spectral resolution (m)	Landsat9 Band N.	Band Center (µm)	Spectral resolution (m)
1- VNIR	0.556	15	1	0.443	60	1- Coastal arosol	0.443	30
2- VNIR	0.661	15	2	0.490	10	2- Blue	0.482	30
3N- VNIR	0.807	15	3	0.560	10	3- Green	0.562	30
3B- VNIR	0.804	15	4	0.665	10	4- Red	0.655	30
4- SWIR	1.656	30	5	0.705	20	-	-	-
5- SWIR	2.167	30	6	0.740	20	-	-	-
6- SWIR	2.209	30	7	0.783	20	-	-	-
7- SWIR	2.262	30	8	0.842	10	-	-	-
8- SWIR	2.336	30	8A	0.865	20	5- NIR	0.865	30
9- SWIR	2.400	30	9	0.945	60	-	-	-
10- TIR	8.291	90	10	1.380	60	9-Cirus	1.375	30
11- TIR	8.634	90	11	1.610	20	6- SWIR1	1.61	30
12- TIR	9.075	90	12	2.190	20	7- SWIR2	2.20	30
13- TIR	10.657	90	-	-	-	8- Panchromatic	0.59	15
14- TIR	11.318	90	-	-	-	-	-	-

Table 2. Characteristics of ASTER, Landsat 9, and Sentinel 2A data.

3.3. Investigation of mineralization trend

According to previous studies and discoveries, 24 primary and secondary ore deposits were Specified in the study area, which was first identified by Dimitrijevic, Yugoslavian team (Dimitrijevic 1973; Honarmand, 2012). These point data had certain dispersion and were analyzed through the Fry method in DotProc software. Fry

analysis is a geometric method for analyzing spatial point data which can be employed as a useful technique for studying mineralization trends (Fry, 1979). In this method, based on the grade assessment at various points of the deposits in the study area, each point is considered as a center, and other points are transferred accordingly. Therefore, all the points of interest are plotted and numbered on a sheet. A point is considered as the center on this sheet and this central point is placed on point number 1. While ensuring that the edges of the two sheets remain parallel and the angles do not change, other points are drawn, and this process continues until the last point (Fry, 1979). Using Fry's analysis, a rose diagram is created, which determines the general direction of mineralization in the study area.

4. Results and Discussion

Many studies have been conducted to enhance hydrothermal alterations in the study area. They mostly discriminate hydrothermal alterations through spectral and statistical techniques (Pour AB and Hashemi 2011., Honarmand, 2012., Hosseinjanizadeh, 2014a, b, Mars JL2014, Hosseinjanizadeh et al., 2017, 2023;). This study used the IDL and logic algorithm (Table 1) to enhance hydrothermal alteration zones. Figure 4 (a) depicts the discriminated hydrothermal alteration zones based on a logical algorithm applied to ASTER data (Table 1). According to this figure, the alteration zones of porphyry copper deposits, including phyllic, argillic, and propylitic alterations, were detected in Sarcheshmeh, Seridon, Sarkooh, Darehzar, Kuh Panj, and Hosseinabad. Furthermore, Sarcheshmeh, Seridune, Darehzar, and Kuh Panj had the highest enhancements. According to the results, Hydrothermal alteration zones are concentrically zoned so that the phyllic alteration is situated at the center, with argillic and propylitic being around the center in most deposits such as; Sarcheshmeh, Seridune, Darehzar, and Kuh Panj Figure 4(a). This pattern is similar to the classic (Lowell and Guilbert,1970) model and was also confirmed in the studies by (Hosseinjanizadeh et al., 2014). Figure 4b illustrates the lineament density in the study area. The location of the characteristic deposits is overlaid on the lineament density to evaluate the conformation of the mineralization trend to the lineament trend. Results revealed good conformation between the zones of the highest lineament densities, characteristic deposits, and hydrothermal alterations. According to Figure 4(b), twenty-one of the twenty- two mineral deposits were situated in high-density zones. This verifies the strong association of the fault density with the porphyry and vein copper indices.

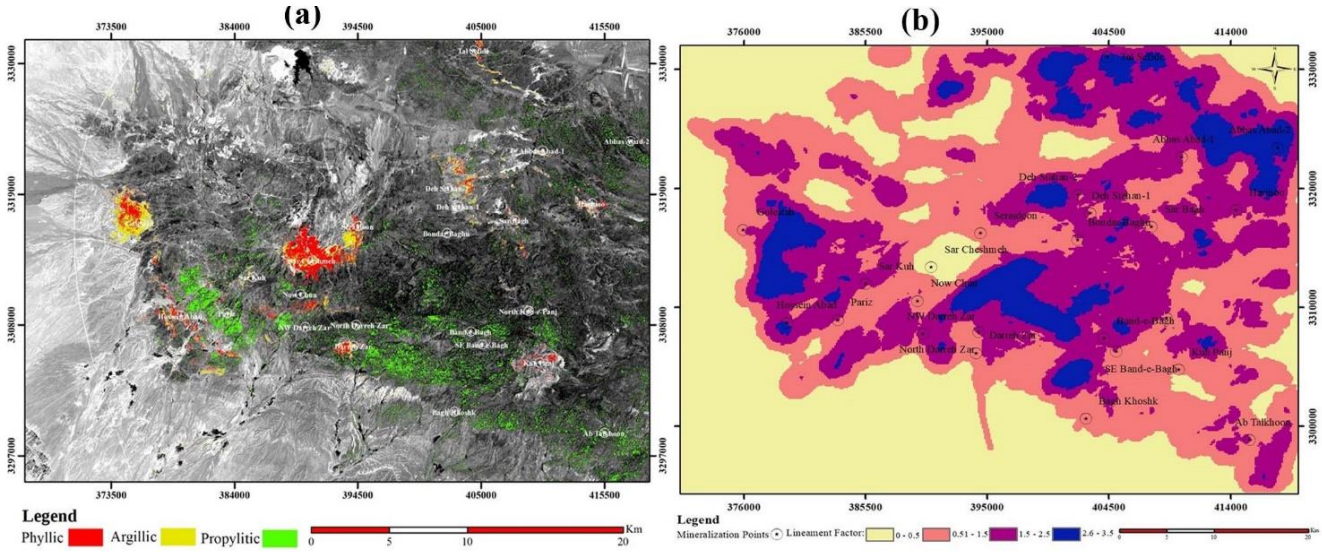

Figure 4. (a) The results of this logical algorithm applied to ASTER data, (b) the lineament density at the study area.

Figure 5 (a) shows the manually extracted lineaments and the locations of the deposits in the region. The porphyry and vein copper indices based on previous works (Dimitrijevic, 1973; Honarmand, 2012) are Sarcheshmeh, Darehzar, Nochon, Sarkooh, Seridune, Bagh-e Khoshk, Ab Talkhoon, Hoseinabad, Deh Siahan1, Kuh Panj, Deh Siahan 2, Bardar Baghoo, Sarbagh, Golestan, Pariz, Tale Sefid, Abbasabad 1 and 2, Harino, Band Bagh.

The rose diagrams of the lineament trends in the study area, which were detected through Robson's (1994) method are shown in Figures 5 b, c, and d. The trend of primary faults is northwest-southeast direction Figure 5(c), whereas the trend of overall and secondary faults is northeast-southwest direction Figure 5 (b) and 5 (d). The dominant fault trend was in the secondary fault direction (northeast-southwest), which implies that the secondary faults are more prevalent in the study area. Determining the relationship between the mineral deposits in the area and the known structural elements (faults) greatly aids in identifying the mineralization trend. To evaluate the distribution of characteristic deposits, Fry analysis was implemented. The results from the Fry image were then converted into a rose diagram to reveal the predominant mineralization trend in the study area. The rose diagram from the Fry analysis of the deposits in the study area indicates the distribution trend of the deposits in the northwest-southeast and northeast-southwest directions Figure 5(e). The predominant mineralization trend, according to the rose diagram from the Fry analysis, aligns with the direction of the primary and secondary faults of the region, which is consistent with the rose diagram of the faults in the study area.

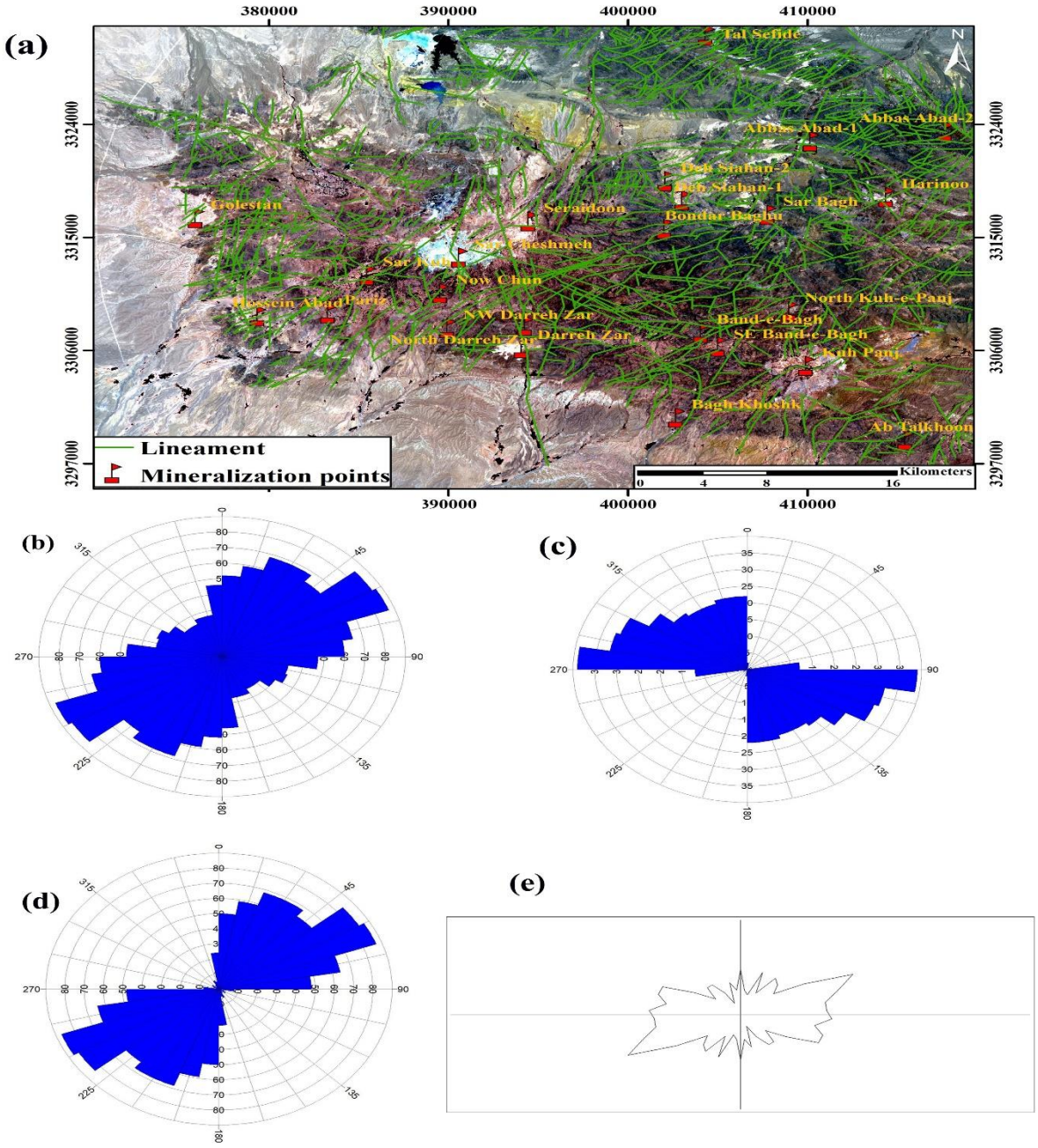

Figure 5. (a) the extracted lineament of the study area which was plotted on Landsat 9 images, (b) a rose diagram of the overall faults, (c) a rose diagram of the primary faults, (d) a rose diagram of the secondary faults, and (e) a rose diagram of mineralization zones detected by Fry analysis

5. Conclusion

In this research, the relationship between hydrothermal alteration zones of porphyry copper deposits and lineament density was investigated in the central part of the Kerman copper belt, Iran, using ASTER, OLI, Sentinel 2, and digital elevation model (DEM) data. ASTER images enhanced hydrothermal alteration zones, including

phyllic, argillic, and propylitic alterations, at key deposits such as Sarcheshmeh, Seridon, Sarkooh, Darehzar, Kuh Panj, and Hosseinabad through a logical algorithm. The results of image processing demonstrated the capability of ASTER images to enhance hydrothermal alterations of porphyry copper deposits. Landsat 9, Sentinel 2, and DEM data accurately enhanced lineaments and faults. Zones with the highest lineament densities showed strong correlations with the identified alteration zones and main deposits in the region. The predominant mineralization trend aligns with the direction of the primary and secondary faults in the northwest-southeast and northeast-southwest directions, respectively. The secondary fault direction (northeast-southwest) was the dominant fault trend, suggesting tectonic influences on mineralization.

6.References

Ahmadfaraj M, Mirmohammadi M, Afzal P, Yasrebi AB, Carranza EJ. Fractal modeling and fry analysis of the relationship between structures and Cu mineralization in Saveh region, Central Iran. Ore Geology Reviews. 2019 Apr 1;107: 172-85.

Alizadeh H, Arian M, Lotfi M, Ghorashi, and M. Ghorbani. "Determination of Porphyry Copper Deposit Locations Using Photo Lineament Factor in Northern Parts of the Dehaj-Sardoiyeh Belt." (2015): 247-252.

Berger BR, Drew LJ. Role of strike-slip duplexes in localization of volcanoes, related intrusions, and epithermal ore deposits. In1997 Annual Meeting of the Geological Society of America 1997.

Beygi S, Talovina IV, Tadayon M, Pour AB. Alteration and structural features mapping in Kacho-Mesqal zone, Central Iran using ASTER remote sensing data for porphyry copper exploration. International Journal of Image and Data Fusion. 2021 Apr 3;12(2):155-75.

Bedini E. The use of hyperspectral remote sensing for mineral exploration: A review. Journal of Hyperspectral Remote Sensing. 2017 Nov;7(4):189-211.

Dimitrijević MD. Geology of Kerman region. Institute for Geological and Mining Exploration and Investigation of Nuclear and Other Mineral Raw Materials; 1973.

Dercourt JE, Zonenshain LP, Ricou LE, Kazmin VG, Le Pichon X, Knipper AL, Grandjacquet C, Sbortshikov IM, Geyssant J, Lepvrier C, Pechersky DH. Geological evolution of the Tethys belt from the Atlantic to the Pamirs since the Lias. Tectonophysics. 1986 Mar 15;123(1-4):241-315.

Emami MH, Mir Mohammad Sadeghi M, Omrani SJ (1993) Magmatic map of Iran (1:2,500,000 scale). Geol Surv Iran.

Fry N. Random point distributions and strain measurement in rocks. Tectonophysics. 1979 Nov 10;60(1-2):89-105.

Greenbaum D. "Review of remote sensing applications to groundwater exploration in basement and regolith." (1985).

Gorokhovich Y, Voustianiouk A. Accuracy assessment of the processed SRTM-based elevation data by CGIAR using field data from USA and Thailand and its relation to the terrain characteristics. Remote sensing of Environment. 2006 Oct 30;104(4):409-15.

Govil H, Gill N, Rajendran S, Santosh M, Kumar S. Identification of new base metal mineralization in Kumaon Himalaya, India, using hyperspectral remote sensing and hydrothermal alteration. Ore Geology Reviews. 2018 Jan 1;92: 271-83.

Guglietta D, Belardi G, Passeri D, Salvatori R, Ubaldini S, Casentini B, Trapasso F. Optimising the management of mining waste by means Sentinel-2 imagery: A case study in Joda West Iron and Manganese Mine (India). Journal of Sustainable Mining. 2020;19(1):4.

Hosienjani Zadeh MH, Tangestani MH, Roldan FV, Yusta I. Sub-pixel mineral mapping of a porphyry copper belt using EO-1 Hyperion data. Advances in Space Research. 2014 Feb 1;53(3):440-51.

Honarmand M, Ranjbar H, Shahabpour J. Combined use of ASTER and ALI data for hydrothermal alteration mapping in the northwestern part of the Kerman magmatic arc, Iran. International Journal of Remote Sensing. 2013 Mar 20;34(6):2023-46.

Honarmand M, Ranjbar H, Shahriari H, Naseri F. Evaluating the effect of using different reference spectra on SAM classification results: an implication for hydrothermal alteration mapping. Journal of Mining and Environment. 2018 Oct 1;9(4):981-97.

Honarmand M. Mineral potential modeling of Kerman metallogenic copper belt using GIS [PhD Thesis]. Kerman: Shahid Bahonar Uni.; 2012.

Hosienjanizadeh M H, Tangestani MH, Roldan FV, Yusta I. Mineral exploration and alteration zone mapping using mixture tuned matched filtering approach on ASTER data at the central part of Dehaj-Sarduiyeh copper belt, SE Iran. IEEE Journal of Selected Topics in Applied Earth Observations and Remote Sensing. 2014a; 7(1):284-9.

Hosseinjanizadeh M, Tangestani MH, Roldan FV, Yusta I, Sub-pixel mineral mapping of a porphyry copper belt using EO-1 Hyperion data. Advance Space Research, 2014b, 53(3):440–451. https:// doi. org/ 10.1016/j. asr. 2013. 11. 029.

Hosseinjanizadeh M, Honarmand M.A remote sensing-based discrimination of high-and low-potential mineralization for porphyry copper deposits; a case study from Dehaj–Sarduiyeh copper belt, SE Iran. European Journal of Remote Sensing. 2017, 50 (1):332-42.

Hosseinjanizadeh M, Honarmand M. Khorasanipour, M., Mapping mining waste and identification of acid mine drainage within an active mining area through sub-pixel analysis on OLI and Sentinel-2. Earth Science Informatics, 2023, 16, 3449–3467.

Iwasaki A, Tonooka H. Validation of a crosstalk correction algorithm for ASTER/SWIR. IEEE Transactions on Geoscience and Remote Sensing. 2005 Nov 21;43(12):2747-51.

Lowell JD, Guilbert JM. Lateral and vertical alteration-mineralization zoning in porphyry ore deposits. Economic geology. 1970 Jul 1;65(4):373-408.

Mars JL. Regional mapping of hydrothermally altered igneous rocks along the Urumieh-Dokhtar, Chagai, and Alborz Belts of western Asia using Advanced Spaceborne Thermal Emission and Reflection Radiometer (ASTER) data and Interactive Data Language (IDL) logical operators: a tool for porphyry copper exploration and assessment. US Geological Survey; 2014.

Mars JC, Rowan LC. Regional mapping of phyllic-and argillic-altered rocks in the Zagros magmatic arc, Iran, using Advanced Spaceborne Thermal Emission and Reflection Radiometer (ASTER) data and logical operator algorithms. Geosphere. 2006 May 1;2(3):161-86.

Molaei M. Investigating structural pattern and alteration for identification of copper mineralization potential using spectral analysis and satellite data processing, case study northern Sarduiyeh Kerman province. Kerman Graduate University of Industrial and Advanced Technology (2020).

Niroumand-Jadidi M, Bovolo F, Bresciani M, Gege P, Giardino C. Water quality retrieval from Landsat-9 (OLI-2) imagery and comparison to sentinel-2. Remote Sensing. 2022 Sep 14;14(18):4596.

Pour AB, Hashim M. Identification of hydrothermal alteration minerals for exploring of porphyry copper deposit using ASTER data, SE Iran. Journal of Asian Earth Sciences. 2011 Nov 11;42(6):1309-23.

Pour AB, Hashim M. Hydrothermal alteration mapping from Landsat-8 data, Sar Cheshmeh copper mining district, south-eastern Islamic Republic of Iran. Journal of Taibah University for Science. 2015 Apr 1;9(2):155-66.

Robson J. The New Zealand national qualifications framework: A basis for action. Journal of further and higher education. 1994 Sep 1;18(3):63-73.

Rowan LC, Mars JC. Lithologic mapping in the Mountain Pass, California area using advanced spaceborne thermal emission and reflection radiometer (ASTER) data. Remote sensing of Environment. 2003 Mar 1;84(3):350-66.

Stocklin J, Nabavi MH. Tectonic map of Iran. Geological Survey of Iran. 1973;1(5).

Samani B. Distribution, setting and metallogenesis of copper deposits in Iran. Porphyry and Hydrothermal Copper & Gold Deposits: A Global Perspective. PGC Publishing, Adelaide. 1998 Nov 30:151-74.

Saric V, Mijalkovic N (1973) Metallogenic map of the Kerman region, 1:500000 scale. In: Exploration for ore deposits in Kerman region. Geol Surv Iran Rep 53:247.

Sabins FF. Remote sensing for mineral exploration. Ore geology reviews. 1999 Sep 1;14(3-4):157-83.

Shirazi A, Hezarkhani A, Pour AB. Fusion of lineament factor (Lf) map analysis and multifractal technique for massive sulfide copper exploration: The Sahlabad area, East Iran. Minerals. 2022 Apr 28;12(5):549.

Shirmard H, Farahbakhsh E, Beiranvand Pour A, Muslim AM, Müller RD, Chandra R. Integration of selective dimensionality reduction techniques for mineral exploration using ASTER satellite data. Remote Sensing. 2020 Apr 16;12(8):1261.

Shahriari H, Honarmand M, Ranjbar H. Comparison of multi-temporal ASTER images for hydrothermal alteration mapping using a fractal-aided SAM method. International Journal of Remote Sensing. 2015 Mar 4;36(5):1271-89.

Shafiei B, Haschke M, Shahabpour J. Recycling of orogenic arc crust triggers porphyry Cu mineralization in Kerman Cenozoic arc rocks, southeastern Iran. Mineralium Deposita. 2009 Apr;44: 265-83.

Shafiei B. Lead isotope signatures of the igneous rocks and porphyry copper deposits from the Kerman Cenozoic magmatic arc (SE Iran), and their magmatic-metallogenetic implications. Ore Geology Reviews. 2010 Oct 1;38(1-2):27-36.

Vialon P, Houchmand-Zadeh A, Sabzehi M. Proposition d'un modele de l'evolution petrostructurale de quelques montagnes iraniennes comme une consequence de la tectonique des plaques. Geol. Congr. sect. 1972;3: 196-208

Van der Werff H, Van der Meer F. Sentinel-2A MSI and Landsat 8 OLI provide data continuity for geological remote sensing. Remote sensing. 2016 Oct 25;8(11):883.

Wang Z, Zhou C, Qin H. Detection of hydrothermal alteration zones using ASTER data in Nimu porphyry copper deposit, south Tibet, China. Advances in Space Research. 2020 Apr 1;65(7):1818-30.

Yousefi SJ, Ranjbar H, Alirezaei S, Dargahi S, Lentz DR. Comparison of hydrothermal alteration patterns associated with porphyry Cu deposits hosted by granitoids and intermediate-mafic volcanic rocks, Kerman Magmatic Arc, Iran: Application of geological, mineralogical and remote sensing data. Journal of African Earth Sciences. 2018 Jun 1;142: 112-23.

Yaghoubpour AA, Hassannejad AA. The spatial distribution of some chromite deposits in Iran, using Fry analysis, (2006): 147-152.